Diagonal Implicit Multigrid Algorithm for the Euler Equations

David A. Caughey*
Cornell University, Ithaca, New York

A multigrid implementation of the Alternating Direction Implicit algorithm has been developed to solve the Euler equations of inviscid, compressible flow. The equations are approximated using a finite-volume spatial discretization with added dissipation provided by an adaptive blend of second and fourth differences. For computational efficiency, the equations are diagonalized by a local similarity transformation so that only a decoupled system of scalar pentadiagonal systems need be solved along each line. Results are computed for transonic flows past airfoils and include pressure distributions to verify the accuracy of the basic scheme and convergence histories to demonstrate the efficiency of the method.

I. Introduction

THE explicit multistage Runge-Kutta method developed by Jameson, Schmidt, and Turkel[1] has proved an effective tool for solving finite-volume approximations to the Euler equations of compressible flow, particularly in the transonic speed regime. The further development of that method within the framework of the multigrid algorithm[2] has made calculations for realistic three-dimensional configurations practical. Attempts to extend the method to solve the Navier-Stokes equations have met with only limited success, however. Although the Runge-Kutta time-stepping algorithm seems still to be suitable, attempts at incorporating the multigrid algorithm have not been particularly successful.[3] The failure of the multigrid method seems to be caused not by the additional complexity of the Navier-Stokes equations themselves but rather by the need to compute solutions on highly-stretched grids in order to resolve the thin shear layers, which appear in solutions at the high Reynolds numbers of practical interest. This requires grids having mesh cells of extremely high aspect ratio near solid boundaries, and the explicit multigrid method does not converge well in this situation, even for the Euler equations.[4]

Physically, this can be attributed to the fact that the time step of the explicit method is limited by the time required for wave propagation across the short dimension of the cell, which can be many times smaller than that required for wave propagation across the long dimension.

In an attempt to circumvent the problem of slow convergence of explicit methods associated with mesh cells of high aspect ratio, an Alternating Direction Implicit (ADI) multigrid method has been developed. The ADI scheme has proven to be a very effective smoothing algorithm for multigrid calculations of transonic flow based upon the steady potential equation.[5]

A method related to the present scheme has also been studied recently by Jameson and Yoon.[6] In order for the implicit method to be an effective smoothing algorithm when used in conjunction with the multigrid algorithm, it is important to include an accurate representation of the dissipative terms. These usually include fourth differences to maintain high accuracy, and their inclusion in the implicit operator requires the inversion of pentadiagonal systems for each one-dimensional factor. To avoid the high cost of solving block pentadiagonal systems, the equations in the present scheme are first diagonalized at each point using a local similarity transformation, following Chaussee and Pulliam.[7] This has the effect of decoupling the equations and requiring the solution of four scalar pentadiagonal equations for each factor in two-dimensional problems. The resulting method has good high wave-number damping, and so it is a good smoothing algorithm for use in conjunction with the multigrid method. It is also computationally efficient because of the need to solve only scalar systems. Additional computational work is required to determine the local similarity transformations and to perform matrix multiplies of the residual and of the intermediate and final corrections, but this is a small fraction of the work required to solve the block systems. In addition, the calculation of the elements of the modal matrices (and their inverses) and the matrix-vector multiplies can be vectorized for each line to reduce further the required CPU time on many computers.

In the following section the method will be described, focusing on those aspects relevant to the implementation of the implicit algorithm. Results of a stability (convergence) analysis will then be presented for a model scalar equation and will illustrate the beneficial high wave-number characteristics of fourth-order implicit schemes. Finally, results for the two-dimensional transonic flow past airfoils will be presented to demonstrate the promise of the method.

II. Analysis

Finite-Volume Formulation

The Euler equations of inviscid compressible flow can be written (in two space dimensions) as

$$\frac{\partial w}{\partial t} + \frac{\partial f}{\partial x} + \frac{\partial g}{\partial y} = 0 \tag{1}$$

where

$$w = \{\rho, \rho u, \rho v, e\}^T \tag{2a}$$

Presented as Paper 87-0354 at the AIAA 25th Aerospace Sciences Meeting, Reno, NV, Jan. 12-15, 1987; received March 23, 1987; revision received Oct. 27, 1987.

*Professor, Sibley School of Mechanical and Aerospace Engineering. Associate Fellow AIAA.

is the vector of conserved dependent variables, and

$$f = \{\rho u,\ \rho u^2 + p,\ \rho uv,\ (e + p)u\}^T \tag{2b}$$

$$g = \{\rho v,\ \rho uv,\ \rho v^2 + p,\ (e + p)v\}^T \tag{2c}$$

are the flux vectors in the x- and y-coordinate directions, respectively. Here ρ and p are the fluid density and pressure, u and v are the velocity components in the x- and y-directions, and e is the total energy per unit volume. For a calorically perfect gas, the pressure is related to the total energy by the equation of state

$$p = (\gamma - 1)\left\{e - \rho\frac{u^2 + v^2}{2}\right\} \tag{3}$$

where γ is the ratio of specific heats.

The present algorithm is implemented within a finite-volume framework to allow the treatment of essentially arbitrary geometries. Under any nonsingular tranformation of independent variables the equations can be written

$$\frac{\partial W}{\partial t} + \frac{\partial F}{\partial \xi} + \frac{\partial G}{\partial \eta} = 0 \tag{4}$$

where $W = hw$ is the transformed dependent variable and

$$F = \{\rho hU,\ \rho hUu + y\eta p,\ \rho hUv - x\eta p,\ (e + \mathrm{p})hU\}^T \tag{5a}$$

$$G = \{\rho hV,\ \rho hVu - y\xi p,\ \rho hVv + x\xi p,\ (e + p)hV\}^T \tag{5b}$$

are the transformed flux vectors. Here $h = x\xi y\eta - x\eta y\xi$ is the determinant of the Jacobian of the transformation (that corresponds to the cell area), and U and V are the contravariant components of the velocity given by

$$h\{U,\ V\}^T = \begin{pmatrix} y\eta u - x\eta v \\ -y\xi u + x\xi v \end{pmatrix} \tag{6}$$

In a finite-volume method, the spatial derivatives are approximated by evaluating the net flux across the faces of each mesh cell using constant values of the velocities on each face. In the present method, the dependent variables are defined at the cell centers; alternatively, these values can be considered as averages for the cell. The value on each face is taken to be the average of the cells sharing the face, so that, for example,

$$(\rho \mathrm{hU})_{i+\frac{1}{2},j} = \tfrac{1}{2}\{(y_{i+\frac{1}{2},j+\frac{1}{2}} - y_{i+\frac{1}{2},j-\frac{1}{2}})(\rho u_{i+1,j} + \rho u_{i,j})$$

$$- (x_{i+\frac{1}{2},j+\frac{1}{2}} - x_{i+\frac{1}{2},j-\frac{1}{2}})(\rho v_{i+1,j} + \rho v_{i,j})\} \tag{7}$$

This approximation is equivalent to a centered difference scheme that is second-order accurate in the mesh spacing in the physical domain when the mesh is smooth.

Artificial Dissipation

In order to prevent the decoupling of the solution at odd- and even-numbered cells in the grid, dissipative terms must be added. Following Jameson,[8] the dissipative terms are constructed as an adaptive blend of second and fourth differences. As pointed out by Jameson, the fourth-difference terms are necessary if the scheme is to converge to a steady state, while the second-difference terms are necessary to prevent excessive oscillation of the solution in the vicinity of shock waves.

The difference approximation, including the dissipative terms, can be written

$$(\mathrm{d}W_{i,j}/\mathrm{d}t) + Qw_{i,j} - Dw_{i,j} = 0 \tag{8}$$

where Q is an operator representing the differences introduced by approximations of the form of Eq. (7) for the fluxes, and D is an operator representing the dissipative terms, which will now be defined. The dissipative operator can be written

$$Dw = D_\xi w + D_\eta w \tag{9}$$

where

$$D_\xi w = \delta_\xi(d_\xi w) \tag{10a}$$

$$D_\eta w = \delta_\eta(d_\eta w) \tag{10b}$$

where $\delta_\xi$and δ_η are central-difference operators spanning a single mesh cell and

$$d_\xi w = \{\epsilon^{(2)}\delta_\xi - \epsilon^{(4)}\delta_\xi^3\}w \tag{11}$$

The coefficients $\epsilon^{(2)}$ and $\epsilon^{(4)}$ are adapted to the solution and are defined as follows.

Let

$$\nu_{i,j} = \frac{|p_{i+1,j} - 2p_{i,j} + p_{i-1,j}|}{p_{i+1,j} + 2p_{i,j} + p_{i-1,j}} \tag{12}$$

then

$$\epsilon^{(2)}_{i+\frac{1}{2},j} = (h/\Delta t^*)_{i+\frac{1}{2},j}\kappa^{(2)} \max(\nu_{i+1,j},\ \nu_{i,j}) \tag{13a}$$

and

$$\epsilon^{(4)}_{i+\frac{1}{2},j} = \max\ [0, (h/\Delta t^*)_{i+\frac{1}{2},j}\kappa^{(4)} - \epsilon^{(2)}_{i+\frac{1}{2},j}] \tag{13b}$$

where $\kappa^{(2)}$ and $\kappa^{(4)}$ are suitably chosen constants, and Δt^* is a time-step scaled to the local Courant number for the cell. The dissipative terms corresponding to the operator D_η are similarly defined. This tailoring of the dissipative coefficients simultaneously activates the second-difference terms and turns off the fourth-difference terms near shock waves, allowing them to be captured with little or no overshoot.

The scaling of the dissipative terms with $1/\Delta t^*$ makes them proportional to the propagation speed of the characteristic that limits the time-step. In the formulation of Jameson,[8] the value of Δt^* is chosen to be the time-step corresponding to a unit Courant number for the cell, defined as

$$\Delta t^* = \frac{\Delta t_\xi \Delta t_\eta}{\Delta t_\xi + \Delta t_\eta} \tag{14}$$

where Δt_ξ and Δt_η are the time-steps corresponding to unit Courant number for one-dimensional problems in the ξ- and η-directions, respectively. Thus, the same value of Δt^* is used to scale the dissipative terms in both coordinate directions. In the present work, it has been found that stability can be maintained while introducing less spurious dissipation if Δt^* is defined differently for the ξ- and η-directions, using Δt_ξ for the determination of d_ξ and Δt_η for the determination of d_η. In a sense, this strategy allows the use of the minimum dissipation to stabilize the one-dimensional problems in each of the coordinate directions, rather than using the larger of the two values of $1/\Delta t$, which is approximately what the Jameson strategy does for large aspect-ratio cells.

It has been found in the present work that somewhat larger values of $\kappa^{(2)}$ and $\kappa^{(4)}$ than those typically used by Jameson are required to prevent significant spurious oscillations of the entropy. The values generally used in the present calculations are $\kappa^{(2)} = 2$ and $\kappa^{(4)} = 1/32$, respectively. When using these larger values, excessive dissipation was introduced in the vicinity of the airfoil surface when the original form of the dissipation was used.

Finally, it should be pointed out that the present formulation of the dissipative terms differs in one other respect from that of Jameson. As shown in Eq. (11), the dissipation included in the energy equation is applied to the energy e, not to the total enthalpy $e+p$. This means that the difference equations can no longer capture identically a constant total enthalpy, and it becomes more difficult to include enthalpy damping into the iterative scheme. However, it was thought more important in the present work to keep the contribution of the dissipation terms in diagonal form.

Iterative Scheme

In smooth regions of the flow, Eqs. (4) plus the dissipative terms just described can be considered approximations to the quasilinear system

$$\frac{\partial W}{\partial t}+A\frac{\partial W}{\partial \xi}+B\frac{\partial W}{\partial \eta}=\frac{\partial}{\partial \xi}\left\{\epsilon^{(2)}\frac{\partial w}{\partial \xi}-\epsilon^{(4)}\frac{\partial^3 w}{\partial \xi^3}\right\}+\frac{\partial}{\partial \eta}\left\{\epsilon^{(2)}\frac{\partial w}{\partial \eta}-\epsilon^{(4)}\frac{\partial^3 w}{\partial \eta^3}\right\} \tag{15}$$

where $A=\{\partial f/\partial W\}$ and $B=\{\partial G/\partial W\}$ are the Jacobians of the transformed flux vectors with respect to the solution. The elements of these matrices can be expressed explicitly in terms of w and the elements of the Jacobian matrix of the coordinate transformation and are given by Warming, Beam, and Hyett[9] and by Chaussee and Pulliam.[7]

Block ADI methods for the equations of compressible gasdynamics were first introduced by Briley and McDonald[10] and by Beam and Warming.[11] The basis of these methods is to approximate the spatial derivatives as weighted averages of differences taken at the old and new time levels, linearizing the changes in the flux vectors using Taylor-series expansions in time, then to approximate the implicit operator as a product of one-dimensional factors. The linearization of the flux vectors is given by

$$\boldsymbol{F}_{i,j}^{n+1}=\boldsymbol{F}_{i,j}^{n}+A_{i,j}^{n}\Delta \boldsymbol{W}_{i,j}^{n}+O(\Delta t^2) \tag{16a}$$

$$\boldsymbol{G}_{i,j}^{n+1}=\boldsymbol{G}_{i,j}^{n}+B_{i,j}^{n}\Delta \boldsymbol{W}_{i,j}^{n}+O(\Delta t^2) \tag{16b}$$

where

$$\Delta \boldsymbol{W}_{i,j}^{n}=\boldsymbol{W}_{i,j}^{n+1}-\boldsymbol{W}_{i,j}^{n}$$

is the correction to be added to the solution in the i,j cell in going from the n to the $n+1$ time level. This gives a scheme of the form

$$\{I+\theta\Delta t[A_{i,j}\delta_\xi+B_{i,j}\delta_\eta-\epsilon_{i,j}^{(2)}(\delta_\xi^2+\delta_\eta^2)(1/h)+\epsilon_{i,j}^{(4)}(\delta_\xi^4+\delta_\eta^4)\times(1/h)]\}^n\Delta \boldsymbol{W}_{i,j}^{n}=-\Delta t\{\delta_\xi \boldsymbol{F}_{i,j}+\delta_\eta \boldsymbol{G}_{i,j}-\epsilon_{i,j}^{(2)}(\delta_\xi^2+\delta_\eta^2)w+\epsilon_{i,j}^{(4)}(\delta_\xi^4+\delta_\eta^4)w\}^n \tag{17}$$

where θ is a parameter determining the degree of implicitness of the scheme (with $0\le\theta\le 1$, where $\theta=1$ corresponds to a fully implicit scheme). Note that for simplicity, Eqs. (17) are written as if the coefficients of the ξ- and η-difference dissipation terms were the same. They are, of course, different, depending as they do on the second difference of the pressure in the appropriate coordinate direction, as well as the value of Δt_ξ or Δt_η when the directionally scaled form of dissipation is used. The appropriate values are used in the calculations. Also, at this point in the analysis it is assumed that the dissipative coefficients in the implicit operator are the same as those on the right-hand side of the equation. The generalization allowing these coefficients in the implicit and explicit portions of the operator to be different will be discussed later.

To make the scheme computationally efficient, the operator on the left-hand side of Eqs. (17) is approximated as the product of two one-dimensional factors to give

$$\{I+\theta\Delta t[A_{i,j}^{n}\delta_\xi-\epsilon_{i,j}^{(2)}\delta_\xi^2(1/h)+\epsilon_{i,j}^{(4)}\delta_\xi^4(1/h)]\}\times\{I+\theta\Delta t[B_{i,j}^{n}\delta_\eta-\epsilon_{i,j}^{(2)}\delta_\eta^2(1/h)+\epsilon_{i,j}^{(4)}\delta_\eta^4(1/h)]\}\Delta \boldsymbol{W}_{i,j}^{n}=-\Delta t\{\delta_\xi \boldsymbol{F}_{i,j}+\delta_\eta \boldsymbol{G}_{i,j}-\epsilon_{i,j}^{(2)}(\delta_\xi^2+\delta_\eta^2)w+\epsilon_{i,j}^{(4)}(\delta_\xi^4+\delta_\eta^4)w\}^n \tag{18}$$

The solution of Eqs. (18) is achieved in two steps. First, the intermediate correction

$$\Delta \boldsymbol{W}_{i,j}^{*}=\{I+\theta\Delta t[B_{i,j}^{n}\delta_\eta-\epsilon_{i,j}^{(2)}\delta_\eta^2(1/h)+\epsilon_{i,j}^{(4)}\delta_\eta^4(1/h)]\}\Delta \boldsymbol{W}_{i,j}^{n} \tag{19a}$$

is determined by solving

$$\{I+\theta\Delta t[A_{i,j}^{n}\delta_\xi-\epsilon_{i,j}^{(2)}\delta_\xi^2(1/h)+\epsilon_{i,j}^{(4)}\delta_\xi^4(1/h)]\}\Delta \boldsymbol{W}_{i,j}^{*}=\boldsymbol{R}_{i,j} \tag{19b}$$

where $\boldsymbol{R}_{i,j}$ is the residual vector corresponding to the right-hand side of Eqs. (18). Thus, to advance the solution one time-step, Eqs. (19) require the solution of one block pentadiagonal system along each line of constant η, followed by the solution of one block pentadiagonal system along each line of constant ξ. The size of the blocks is 4×4 for this two-dimensional problem; for a three-dimensional problem, there are three factors to be inverted, and the blocks are 5×5.

The scheme described by Eqs. (19) would be reasonably efficient if it were not necessary to add numerical dissipation to stabilize the central-difference approximation. In particular, if only second-difference terms were added (i.e., if $\epsilon^{(4)}=0$), it would still be necessary only to solve block tridiagonal systems. However, as pointed out above, the inclusion of fourth differences is essential if the solution is ultimately to converge to a steady state, and it is important to treat these differences implicitly if the solution is to converge rapidly.[12] This can be done in a straightforward manner, following the development above, but leads to a requirement to solve block pentadiagonal systems for each factor. This requires approximately twice the computational labor of the block tridiagonal inversions and begins to become computationally prohibitive.

An alternative is to diagonalize the equations at each mesh point, yielding a decoupled set of equations, each of which can be solved using a scalar pentadiagonal solver. This requires approximately one-quarter the computational labor of the block pentadiagonal solution (and requires, in fact, only about half the work required to solve the block tridiagonal systems). Let Q_A and Q_B be the modal matrices of the Jacobians A and B, so that $Q_A^{-1}AQ_A=\Lambda_A$ and $Q_B^{-1}BQ_B=\Lambda_B$ are diagonal matrices whose nonzero elements are the eigenvalues of A and B, respectively. At each point the linearized equations can then be written

$$\{I+\theta\Delta t[\Lambda_{A_{i,j}^{n}}\delta_\xi-\epsilon^{(2)}\delta_\xi^2(1/h)+\epsilon^{(4)}\delta_\xi^4(1/h)]\}Q_{A_{i,j}^{n}}^{-1}\times Q_{B_{i,j}^{n}}\{I+\theta\Delta t[\Lambda_{B_{i,j}^{n}}\delta_\eta-\epsilon^{(2)}\delta_\eta^2(1/h)+\epsilon^{(4)}\delta_\eta^4(1/h)]\}\Delta \boldsymbol{V}_{i,j}^{n}=-\Delta t Q_{A_{i,j}^{n}}^{-1}\{\delta_\xi \boldsymbol{F}_{i,j}+\delta_\eta \boldsymbol{G}_{i,j}-\epsilon_{i,j}^{(2)}(\delta_\xi^2+\delta_\eta^2)w+\epsilon_{i,j}^{(4)}(\delta_\xi^4+\delta_\eta^4)w\}^n \tag{20}$$

where

$$\Delta \boldsymbol{W}_{i,j}^{n}=Q_B\Delta \boldsymbol{V}_{i,j}^{n}$$

i.e., $\Delta \boldsymbol{V}_{i,j}^{n}$ is the change in the vector of characteristic variables corresponding to the η flux vector. The solution procedure is similar in structure to that of the block scheme. First, the

intermediate correction

$$\Delta V^*_{i,j} = Q^{-1}_{A^n_{i,j}} Q_{B^n_{i,j}} \{I + \theta\Delta t[\Lambda_{B^n_{i,j}}\delta_\eta - \epsilon^{(2)}\delta^2_\eta \times (1/h) + \epsilon^{(4)}\delta^4_\eta(1/h)]\}\Delta V^n_{i,j} \quad (21a)$$

is determined by solving the equations

$$\{I + \theta\Delta t[\Lambda_{A^n_{i,j}}\delta_\xi - \epsilon^{(2)}\delta^2_\xi(1/h) + \epsilon^{(4)}\delta^4_\xi(1/h)]\}\Delta V^*_{i,j} = Q^{-1}_{A^n_{i,j}} R_{i,j} \quad (21b)$$

Then the correction itself is determined by solving Eqs. (21a). As described above, the solution of Eqs. (20) requires the determination of the modal matrices of the A and B Jacobians (and their inverses) at each point, a matrix multiply of the residual vector, the solution of four scalar pentadiagonal systems along each ξ-line, another matrix multiply of the intermediate correction vector, a second set of four scalar pentadiagonal solutions along each η-line, and a final matrix multiply to extract the corrections to the primitive variables. The cost of determining the elements of the modal matrices is about twice that of computing the elements of the Jacobian matrices in the block method, but even with the extra matrix-vector multiplies, the diagonalized procedure is considerably more efficient than solution of the block pentadiagonal systems. The advantage of the diagonal scheme would be even greater on a vector computer, since the determination of the elements of the modal matrices and the additional matrix-vector multiplies are easily vectorizable.

The incorporation of the scheme within the multigrid algorithm is straightforward, following the procedure developed by Jameson.[2] An auxiliary mesh (denoted by the subscript $2h$) is defined by eliminating every second line of the fine grid (denoted by the subscript h), effectively doubling the mesh spacing in each direction. Values of the flow variables are restricted to the coarser grid using area-weighted averages of the form

$$w^{(0)}_{2h} = \sum \frac{S_h w_h}{S_{2h}} \quad (22)$$

where S_h is the area of a fine-grid cell, and the summation is over the fine-grid cells contained in the coarse-grid cell. It is important that the solution on the coarser grid be driven by the residual computed on the fine grid, and so a forcing function is defined as

$$P_{2h} = \sum R_h - R_{2h}(w^{(0)}_{2h}) \quad (23)$$

where R_{nh} is the residual on grid level having grid spacing nh, and $w^{(0)}_{2h}$ is the initial estimate for the solution, restricted from the h grid. The residual used to drive the corrections on the coarser grid is then given by

$$\tilde{R}_{2h} = R_{2h}(w_{2h}) + P_{2h} \quad (24)$$

After corrections have been computed on the coarser grid, the process is continued to still coarser grids in a similar manner. The residual on the next coarser grid is

$$\tilde{R}_{4h} = R_{4h}(w_{4h}) + P_{4h} \quad (25)$$

where

$$P_{4h} = \sum \tilde{R}_{2h} - R_{4h}(w^{(0)}_{4h}) \quad (26)$$

After corrections have been computed on the coarsest grid, they are prolonged back to successively finer grids using bilinear interpolation in the computational coordinates. After the corrections have been added to the solution on the finest grid, the cycle is repeated.

It has been found necessary to update only the body-surface boundary conditions on coarser grids; far-field boundary conditions are frozen during each multigrid cycle.

In the present work, the overall convergence rates seem to be relatively insensitive to the number of time-steps performed at each stage of the multigrid cycle. The best asymptotic rates seem to be obtained using a fixed V-cycle in which one time-step is performed on the finest and on each coarser grid as the grid is coarsened, but no smoothing is performed on the coarser grids after corrections have been added. Since the computational work required per time-step is very nearly proportional to the number of grid cells, the work per time-step on each coarser grid is approximately one-quarter that on the previous grid. Thus, for the above fixed strategy, one multigrid cycle requires slightly less than 4/3 work units, if a work unit is defined as the amount of computation required for one time-step on the fine grid. When the freestream is used as the initial estimate on fine grids, it is sometimes necessary to have more smoothing in the early stages of the iteration. Thus, most of the results to be presented here were computed using an additional smoothing step after corrections have been added to all but the finest grid from still coarser grids. This strategy requires slightly less than 5/3 work units per multigrid cycle.

Since Jameson found it desirable to use only a fixed-coefficient, second-difference form of the dissipation on coarser grids, additional efficiency with the present formulation can also be achieved by using a scalar tridiagonal solver on the coarser grid levels.

Boundary Conditions

The treatment of the explicit boundary conditions in the far field follows that of Jameson,[8] based upon the Riemann invariants of the one-dimensional problem normal to the boundary. The solutions computed to date have involved only subsonic freestream Mach numbers, so the far-field boundaries have either subsonic inflow or outflow. For a boundary of constant η, the Riemann invariants

$$R_1 = \frac{x_\xi v - y_\xi u}{\sqrt{x^2_\xi + y^2_\xi}} + \frac{2c}{\gamma - 1} \quad (27a)$$

$$R_2 = \frac{x_\xi v - y_\xi u}{\sqrt{x^2_\xi + y^2_\xi}} - \frac{2c}{\gamma - 1} \quad (27b)$$

are determined using either freestream values or those extrapolated from the interior, depending upon the direction of propagation of the characteristic. These values are then used to determine the normal component of velocity and the speed of sound at the boundary

$$q_n = \frac{R_1 + R_2}{2} \quad (28a)$$

$$c = \frac{\gamma - 1}{4}(R_1 - R_2) \quad (28b)$$

The velocity component tangential to the boundary is set to the freestream value for inflow or extrapolated from the interior for outflow, as is the entropy of the fluid. The density and pressure are then determined from the speed of sound and the entropy.

At the body surface, only the pressure is required, since the contravariant velocity component normal to the boundary is identically zero there. The pressure at the body surface is determined from the normal momentum equation following the formula proposed by Rizzi.[13] Since the airfoil surface is a line of constant η in the present implementation,

$$(y^2_\xi + x^2_\xi)\frac{\partial p}{\partial \eta} = (x_\xi x_\eta + y_\xi y_\eta)\frac{\partial p}{\partial \xi} + \rho h U(x_{\xi\xi} v - y_{\xi\xi} u) \quad (29)$$

is used to estimate the normal pressure gradient using values of the dependent variables in the row of cells next to the body surface. Then

$$p_{i,1/2} = p_{i,1} - \frac{\Delta\eta}{2}\frac{\partial p}{\partial \eta} \tag{30}$$

is used to determine the pressure on the surface.

As a result of the diagonalization of the ADI scheme, it is straightforward to treat the implicit boundary conditions in a manner consistent with the characteristic theory. From Eqs. (18) and (21b), it is clear that

$$\Delta V^* = Q_A^{-1}\Delta W + O(\Delta t^2) \tag{31a}$$

while from the definition of V

$$\Delta V = Q_B^{-1}\Delta W \tag{31b}$$

Thus, ΔV^* is an approximation to the change in the vector of characteristic variables for the one-dimensional problem in the ξ-direction, whereas ΔV is the change in the vector of characteristic variables for the one-dimensional problem in the η-direction. In the ξ-implicit sweeps, the boundary condition for those elements of ΔV^* corresponding to characteristics entering the domain is taken to be a homogeneous Dirichlet condition, whereas the boundary condition for those elements corresponding to characteristics leaving the domain is taken to be homogeneous Neumann. The boundary conditions for the η-implicit sweeps are treated similarly.

III. Convergence Analysis

The interpolation of corrections from the coarser grids to the finer grids will inevitably introduce error that has high-wave-number content, which cannot be rapidly expelled through the boundaries. For the multigrid algorithm to be efficient, therefore, the smoothing algorithm must be effective at eliminating these high wave-number errors. The high wave-number damping characteristics of the present scheme can be analyzed by studying the application of the ADI scheme to the simple scalar equation

$$\partial w/\partial t + c\partial w/\partial x + c\partial w/\partial y + c\epsilon(\Delta x^3\partial^4 u/\partial x^4 + \Delta y^3\partial^4 u/\partial y^4) = 0 \tag{32}$$

Under the assumption that $\Delta x = \Delta y$, an ADI approximation for this equation can be written

$$\{1 + \theta\lambda[\delta_x + \tilde{\epsilon}\delta_x^4]\}\{1 + \theta\lambda[\delta_y + \tilde{\epsilon}\delta_y^4]\}\Delta w = -\lambda\{\delta_x + \delta_y + \epsilon(\delta_x^4 + \delta_y^4)\}w^n \tag{33}$$

where $\lambda = c\Delta t/\Delta x$ is the Courant number. The amplification factor G in a von Neumann analysis of this scheme is given by

$$\begin{aligned}&\{1 + \lambda\theta(i\sin\xi + 16\tilde{\epsilon}\sin^4\xi/2)\}\{1 + \lambda\theta\\ &\times(i\sin\eta + 16\tilde{\epsilon}\sin^4\eta/2)\}G =\\ &1 + i\lambda(\theta - 1)\{\sin\xi + \sin\eta\} + 16\lambda(\theta\tilde{\epsilon} - \epsilon)\\ &\times\{\sin^4\xi/2 + \sin^4\eta/2\}\\ &+ \lambda^2\theta^2\{-\sin\xi\sin\eta + 256\tilde{\epsilon}^2\sin^4\xi/2\sin^4\eta/2\\ &+ 16i\tilde{\epsilon}(\sin\xi\sin^4\eta/2 + \sin\eta\sin^4\xi/2)\}\end{aligned} \tag{34}$$

where ξ and η are the mesh wave numbers in the x- and y-directions, respectively. The amplification factor can be forced to be zero in the high wave-number limit of $\xi = \eta = \pi$

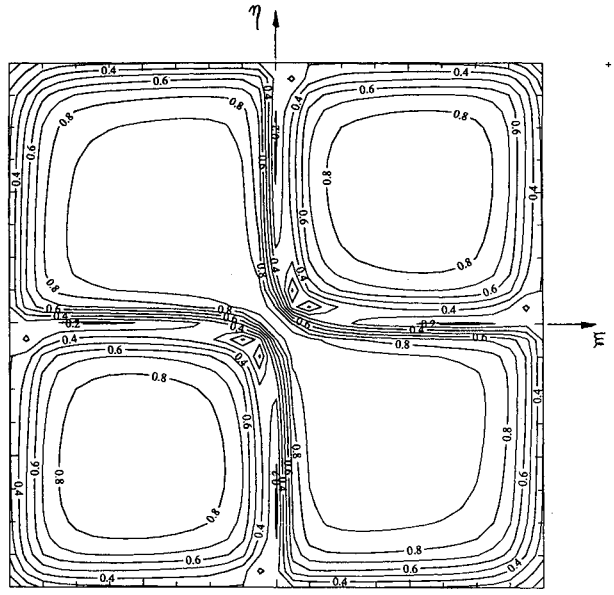

Fig. 1 Growth factor for model hyperbolic equation with fourth-difference dissipation; Jameson-Yoon "optimal" coefficients.

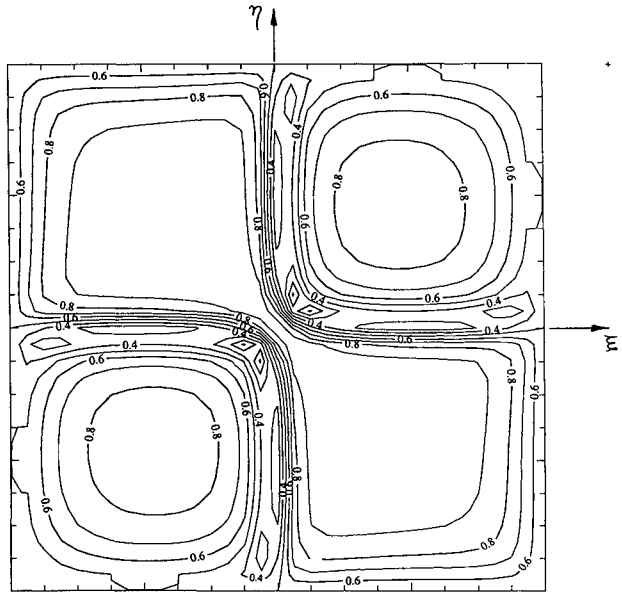

Fig. 2 Growth factor for model hyperbolic equation with $\tilde{\epsilon} = \epsilon$.

by the choice of

$$\tilde{\epsilon} = \frac{\sqrt{32\lambda\epsilon} - 1}{16\lambda\theta} \tag{35}$$

as was noted by Jameson and Yoon.[6] (The typographical error in their formula has been corrected in the above equation.) This is not necessarily the optimal choice for use with the multigrid algorithm, however. Figures 1 and 2 illustrate the variation in the modulus of the amplification factor $|G|$ with mesh wave number in the two coordinate directions. Figure 1 corresponds to the condition of Eq. (35), whereas Fig. 2

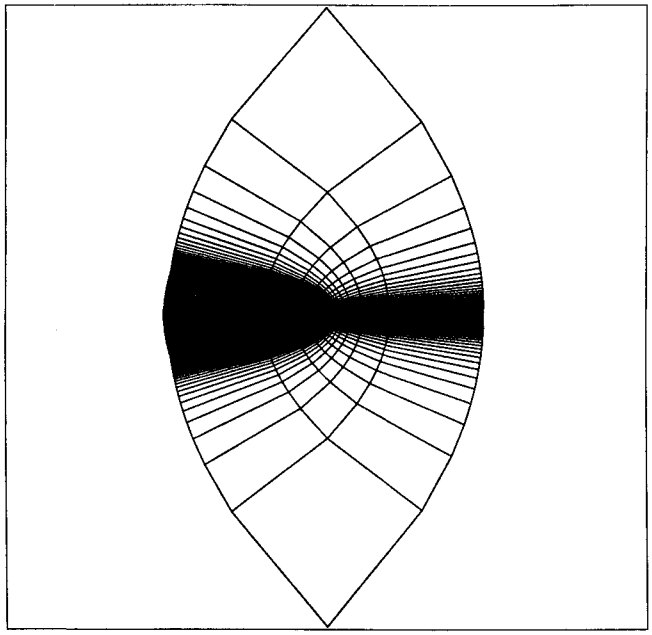

Fig. 3a Far-field structure of 192 × 32 cell C-grid for NACA 0012 airfoil calculation.

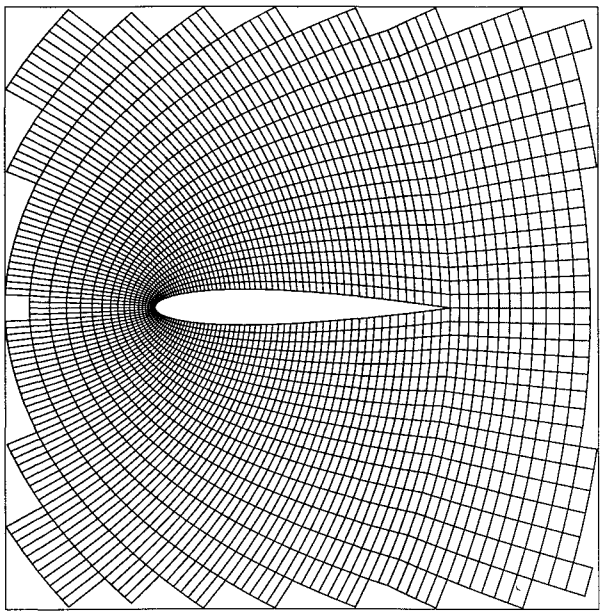

Fig. 3b Structure of 192 × 32 cell C-grid for NACA 0012 airfoil in vicinity of airfoil surface.

corresponds to the choice of $\tilde{\epsilon} = \epsilon$. Although the amplification factor does not go to zero in the high wave-number limit in the latter case, the average damping in the high wave-number region is still quite good. Numerical experiments confirm that there is little reason not to choose $\tilde{\epsilon} = \epsilon$.

IV. Results

The algorithm described above has been applied to the problem of transonic flow past an airfoil. The diagonal-implicit scheme has been coded, including the blended second- and fourth-difference dissipation terms and multigrid implementation. Results have been obtained for a variety of airfoils and freestream conditions to verify the accuracy of the basic algorithm. First, airfoil surface pressure distributions will be presented for several of these cases, then the convergence rates of both the block-implicit and diagonalized schemes will be compared, and the convergence acceleration due to multigrid will be shown. Finally, the entropy variations will be studied to compare the relative amounts of spurious dissipation introduced by the dissipative terms.

All results presented here have been calculated on C-grids containing 192 × 32 grid cells in the wraparound and normal directions, respectively. The far-field boundaries of the grid are located approximately 50 chords upstream and downstream of the airfoil and 100 chords laterally. The entire grid for a NACA 0012 airfoil is shown in Fig. 3a, and the grid structure in the vicinity of the airfoil surface is shown in Fig. 3b. The ratio of largest to smallest cell area is slightly more than eight orders of magnitude. The most elongated cells have aspect ratios of approximately 168 and 115 in the η- and ξ-directions, respectively, and so the ratio of largest to smallest geometric aspect ratio is almost 2×10^4. Most of the calculations were performed on an FPS AP-264 Scientific Processor attached to an IBM 3084 host. A typical calculation (consisting of 100 work units) requires less then 2.4 min of CPU time for the decoupled pentadiagonal implicit scheme, but almost 12.0 min for the pentadiagonal block implicit scheme. The code has also been run on the CRAY X-MP; after modest rearrangement to get most of the nonrecursive parts of the code to vectorize, it was found that 100 work units of the decoupled pentadiagonal scheme required approximately 20 s CPU time.

Airfoil surface pressure distributions for several cases will first be presented to verify the accuracy of the scheme. These calculations were performed with the directionally scaled dissipation and were well enough converged that the final answers are independent of the form of the ADI scheme used. Figure 4a presents the surface pressure distribution for the NACA 0012 airfoil at a freestream Mach number of 0.85 and zero deg angle of attack. The results of the present calculations are compared with those of Jameson and Yoon.[6] As may be seen from the figure, the results are virtually identical. Figure 4b presents similar results for the NACA 0012 airfoil at a freestream Mach number of 0.80 and 1.25 deg angle of attack. The results for this case are compared with those of Pulliam.[12] Here, the agreement is not quite so good as for the previous case, the primary difference being the better resolution of the shock on the airfoil lower surface by Pulliam's scheme. This is a result primarily of the finer grid density used in the Pulliam calculation.

Convergence results will be presented only for the NACA 0012 airfoil at a freestream Mach number of 0.80 and 1.25 deg angle of attack. Convergence rates for other cases are similar. The calculations were performed as strict V-cycles, starting with the undisturbed flow as the initial guess on the fine grid, using the fully implicit scheme ($\theta = 1$). Solutions of a given accuracy can usually be obtained more cheaply using grid sequencing in which multigrid solutions are first obtained on coarser grids, then interpolated for use as initial conditions on finer grids. An example using this strategy will be presented later. The logarithm of the average over all the grid cells of the residual of the continuity equation $|\Delta\rho/\Delta t|$, the total number of grid cells in which the local Mach number is supersonic, and the lift and drag coefficients are plotted as a function of computational labor, measured in work units. The latter three quantities are plotted in arbitrary units, scaled to their final values. These final values are independent of the iterative process and of the parameters used in the iterative process, since the scheme has been cast in delta (or correction) form.

The convergence histories for the present diagonal-implicit scheme on a single grid and with five-level multigrid are shown in Fig. 5a and 5b. The Courant number is different in the two cases, being chosen to give the best asymptotic convergence rates in each case. The Courant number for the single-grid

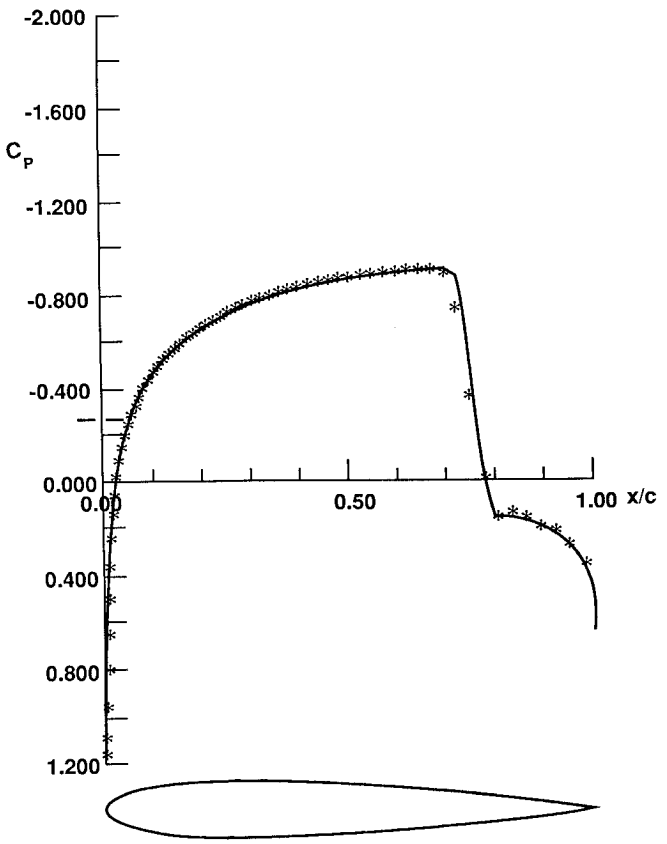

Fig. 4a Surface pressure distribution for NACA 0012 airfoil at 0.85 Mach number and zero deg angle of attack; symbols are present solution, solid line is Ref. 6.

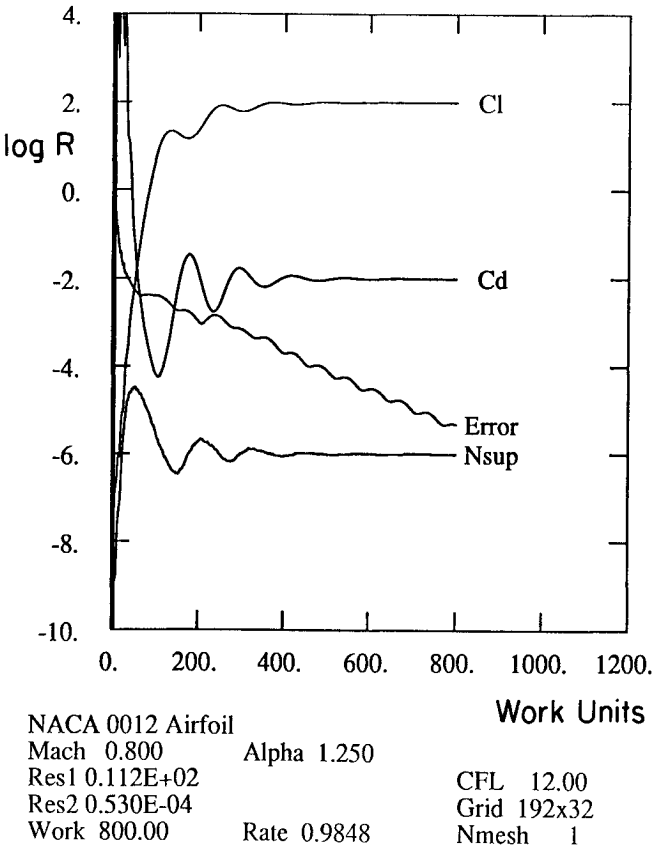

Fig. 5a Convergence history for diagonal-implicit scheme on single grid (local time-stepping is used at Courant number 12).

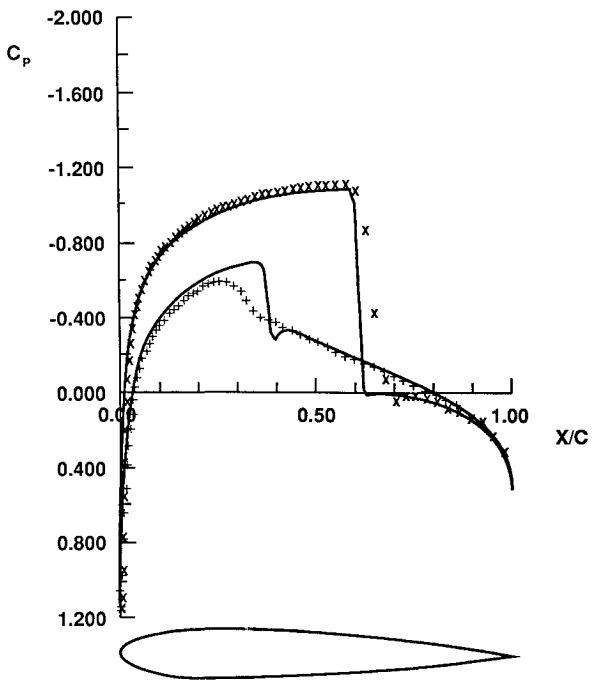

Fig. 4b Surface pressure distribution for NACA 0012 airfoil at 0.80 Mach number and 1.25 deg angle of attack; symbols are present solution, solid line is Ref. 12.

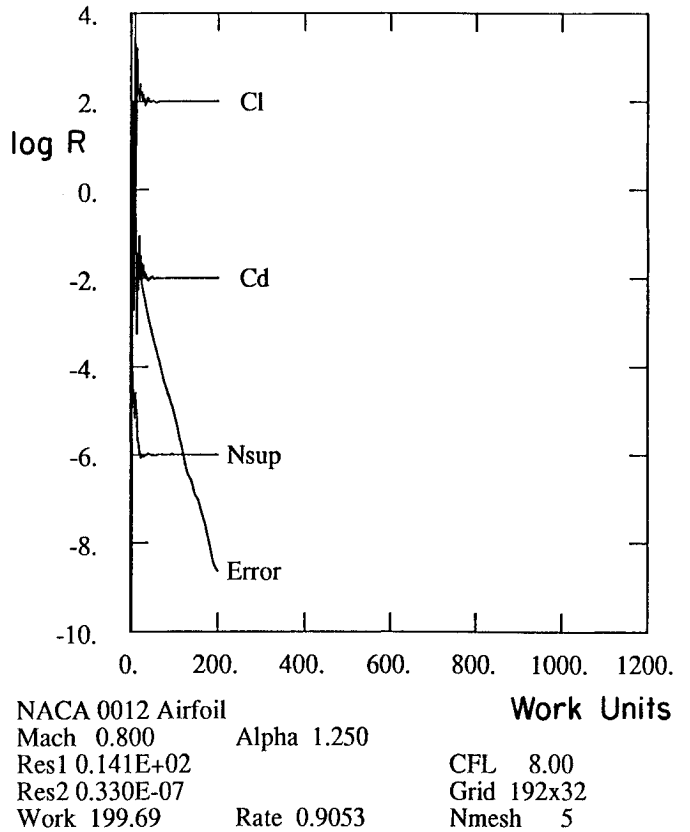

Fig. 5b Convergence history for diagonal-implicit scheme using five-level multigrid (local time-stepping is used at Courant number 8).

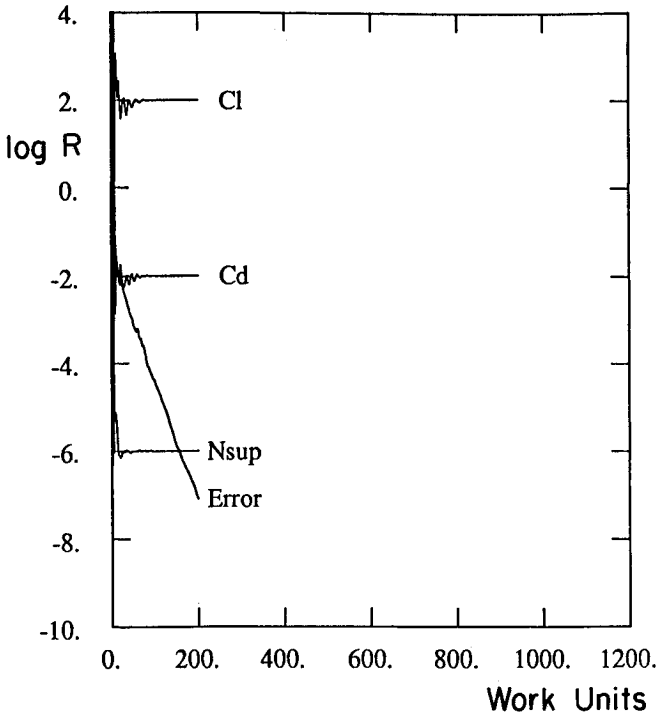

Fig. 5c Convergence history for block-implicit multigrid scheme (local time-stepping is used at Courant number 8).

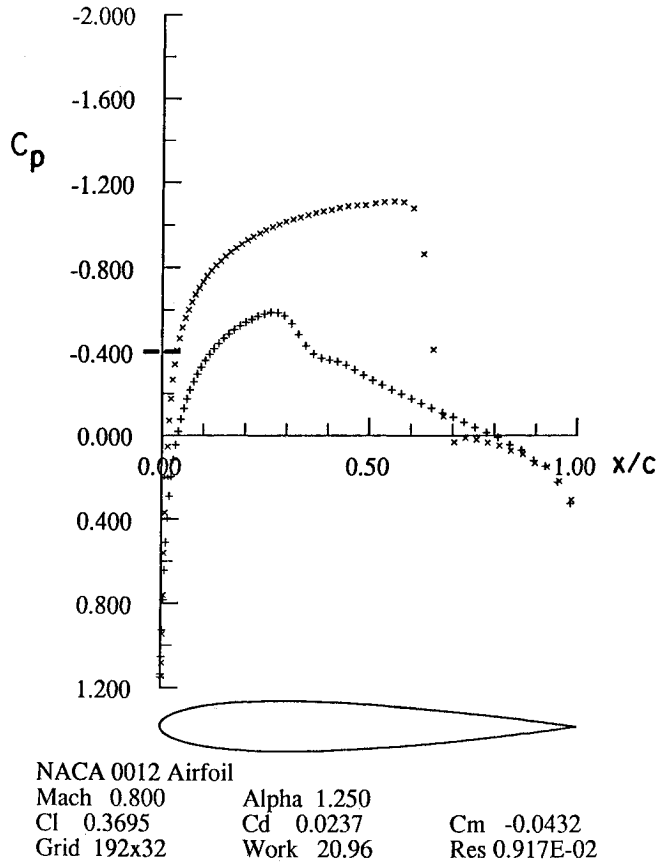

Fig. 6 Surface pressure distribution for NACA 0012 airfoil at 0.80 Mach number and 1.25 deg angle of attack, computed using only 10 multigrid cycles on each of three successively finer grids.

result is 12.0, whereas that for the multigrid result is 8.0. In both cases, local time-stepping has been used, i.e., the time-step in each cell is adjusted to correspond to a fixed Courant number. The scheme remains stable at higher Courant numbers, but the overall convergence rate is degraded because of the poorer high wave-number damping at the larger values of time step. Using multigrid, the average residual in this case has been reduced by almost nine orders of magnitude in 121 multigrid cycles (corresponding to approximately 200 work units); the three measures of global convergence, the number of grid cells in which the local Mach number is supersonic, and the lift and drag coefficients have converged to within plottable accuracy of their final values after only 60 multigrid cycles (corresponding to approximately 99 work units).

Calculations using a tridiagonal version of the diagonalized implicit algorithm (obtained simply by zeroing out the additional coefficients) converge asymptotically nearly as well as the pentadiagonal scheme but suffer from more highly oscillatory convergence. Indeed, for the case presented above, the tridiagonal scheme fails to converge when started from uniform freestream conditions on the fine grid.

Figure 5c presents the convergence history of the implicit multigrid scheme using a block pentadiagonal solver instead of the diagonalized scheme. The asymptotic rate is almost identical to that of the diagonalized scheme, but the diagonal scheme suffers less from oscillation in the force coefficients and in the number of supersonic points early in the calculation. This is probably due to the better treatment of the implicit boundary conditions in the diagonalized scheme, as described earlier. For the block pentadiagonal scheme, the implicit boundary conditions were taken to be homogeneous Dirichlet conditions at both ends of the lines for both factors. Calculations for this flowfield using a block tridiagonal solver failed to converge on the fine grid of this test case; this also was probably due to the poorer representation of the implicit boundary conditions, which were treated as for the block pentadiagonal solver. In any event, the convergence rate does not seem to have been adversely affected by the diagonalization procedure. This fact is also confirmed by the fact that the convergence rates of the present diagonalized scheme are comparable to those of Jameson and Yoon[6] when they used the full block pentadiagonal scheme.

The results presented above were calculated using $\tilde{\epsilon}^{(2)} = \epsilon^{(2)}$ and $\tilde{\epsilon}^{(4)} = \epsilon^{(4)}$. Diagonalized pentadiagonal multigrid calculations have also been performed using the "optimal" coefficients corresponding to Eq. (35). The convergence for these cases tends to be more oscillatory. A comparison for the case presented above is not presented because the scheme diverges when started from uniform freestream conditions (although it does converge when grid sequencing is used).

The above convergence studies have demonstrated that the rate of convergence does not deteriorate with convergence, and that the residuals can be driven to machine zero (corresponding to residuals of approximately 10^{-13} on the above plots for the 64-bit AP 264) in less than 400 work units. Of course, the primary advantage of the multigrid method is its ability to reduce all wave-number components of the error with nearly the same efficiency, and the above plots show that the global measures of convergence (number of supersonic points and force coefficients) converge to plottable accuracy in less than 100 work units. To further emphasize this point, the pressure distribution for the above case is shown in Fig. 6 for a calculation in which grid sequencing was used on three grids. Ten multigrid cycles were performed on grids containing 48 × 8 cells, 96 × 16 cells, and 192 × 32 cells, interpolating

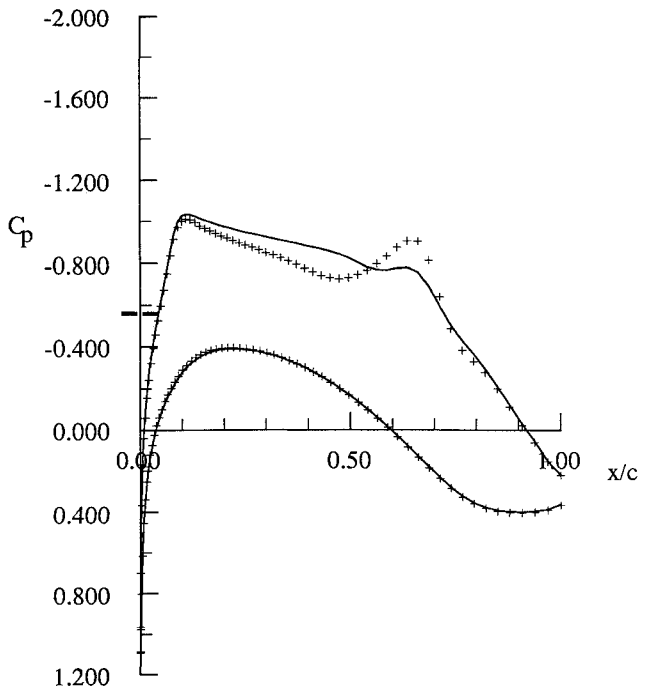

Fig. 7 Surface pressure distribution for Korn airfoil at shock-free design Mach number of 0.75 and 0 deg angle of attack; solid line represents directional form of dissipation, symbols represent conventional form of dissipation.

from the coarser-grid solution to obtain initial estimates for the solution on each finer grid. For this calculation, two smoothing steps were performed on each coarser grid after corrections had been interpolated from yet coarser grids; using this strategy, each multigrid cycle requires slightly less than two work units. The grid sequencing strategy requires a total computational labor that is less than one and one-third times the 20 work units on the finest grid. As can be seen, although the average residual has been reduced by less than 1.5 orders of magnitude, the pressure distribution is virtually identical to that of the fully converged solution of Fig. 4b, and both the lift and drag coefficients agree to three significant figures.

Finally, the results of several calculations with the conventional form of the dissipation will be presented. Calculations for the Korn airfoil at its shock-free design condition and for the NACA 0012 airfoil at a freestream Mach number of 0.80 and 1.25 deg angle of attack are presented. Convergence rates are similar to those presented earlier, so only converged pressure and entropy distributions will be shown. Figure 7 presents the solution for the Korn airfoil. The surface pressure distribution calculated using the directionally scaled dissipation is very nearly shock free; the weak shocklet appearing at the downstream boundary of the supersonic zone is due to the errors introduced by the spatial discretization, including the introduction of the artificial dissipative terms into the difference equations. The shocklet is significantly stronger in the pressure distribution calculated using the original form of the dissipation. This effect is even more pronounced on coarser grids, as might be used in three-dimensional calculations.

The surface pressure distribution for the NACA 0012 airfoil computed using the conventional dissipation is virtually identical to that computed using the directionally scaled form. Figures 8 and 9 present comparisons of the entropy generated for the NACA 0012 case. The variable plotted is

$$s = \frac{p}{\rho^{\gamma}} - 1$$

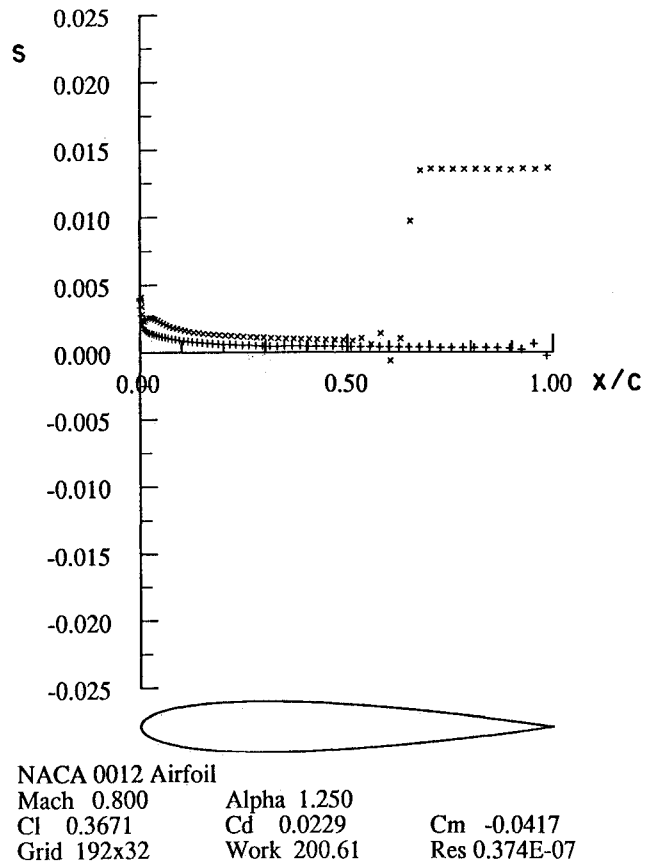

Fig. 8a Surface entropy distribution for NACA 0012 airfoil at 0.80 Mach number and 1.25 deg angle of attack using conventional form of dissipation.

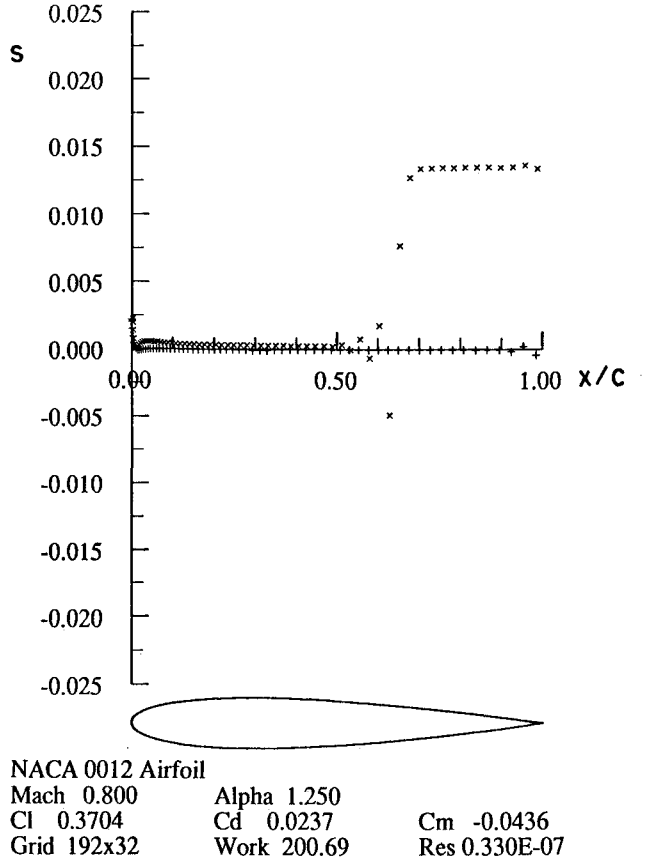

Fig. 8b Surface entropy distribution for NACA 0012 airfoil at 0.80 Mach number and 1.25 deg angle of attack using directionally scaled dissipation.

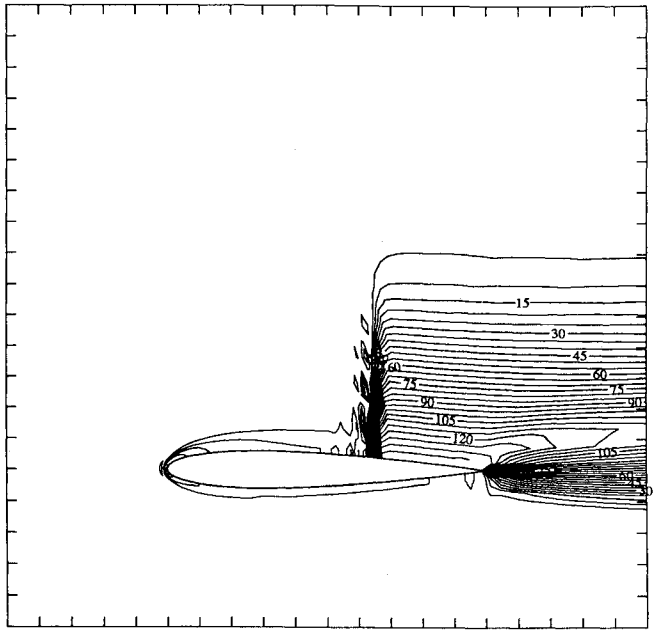

Fig. 9a Contours of constant entropy near NACA 0012 airfoil at 0.80 Mach number and 1.25 deg angle of attack using conventional form of dissipation.

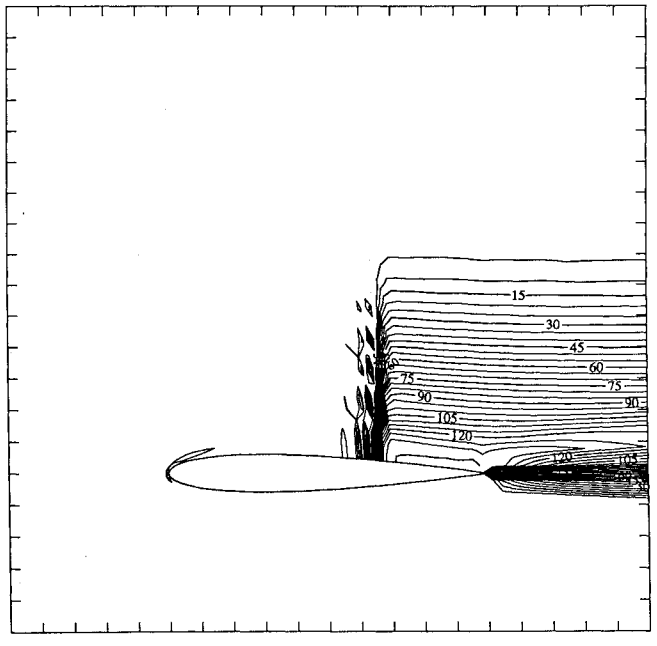

Fig. 9b Contours of constant entropy near NACA 0012 airfoil at 0.80 Mach number and 1.25 deg angle of attack using directionally scaled dissipation.

which is a relative measure of the change in entropy. The value $s = 0$ corresponds to the freestream entropy, since both p and ρ are normalized with respect to their values in the freestream. It is not difficult to show, using the isentropic relations, that the variable s is related to the percentage loss in total pressure by

$$\Delta p_0/p_{0\infty} = 1 - (1 + s)^{-1/(\gamma - 1)}$$

Figures 8a and 8b show the entropy distributions along the airfoil surface for the conventional and directional forms of the dissipation, and Figs. 9a and 9b show contours of constant entropy in the vicinity of the airfoil surface. These clearly show the location of the strong shock wave extending from the upper surface of the airfoil and also show a significantly larger entropy layer extending from the vicinity of the leading edge for the result computed using the conventional dissipation.

V. Conclusions

A multigrid implementation of a diagonalized Alternating Direction Implicit algorithm to solve the Euler equations of inviscid, compressible flow has been described. The equations are approximated using a finite-volume spatial discretization with added dissipation provided by an adaptive blend of second and fourth differences. The diagonalization of the implicit factors to produce scalar pentadiagonal systems results is an appreciable savings in computational labor. Results for transonic flows past airfoils verify the accuracy of the basic scheme, and convergence histories demonstrate the efficiency of the method. The tridiagonal form of the diagonalized scheme produces asymptotic convergence rates nearly as good as the pentadiagonal form but is less robust. The block tridiagonal scheme fails to converge on fine grids, probably due to less well-represented boundary conditions. Comparisons of results calculated with a directionally-scaled numerical dissipation demonstrate its tendency to introduce less spurious entropy than the conventional form. Application of the method to compute flows in high-speed inlets and calculations on the more highly stretched grids typical of high Reynolds number viscous calculations are currently being investigated.

Acknowledgments

This work has been supported by grants from the NASA Lewis Research Center under Grant NAG 3-645 and by the NASA Ames Research Center under Grant NAG 2-373. The computations presented here have been performed at the Cornell National Supercomputer Facility of the Center for Theory and Simulation in Science and Engineering, which is funded in part by the National Science Foundation, New York State, and IBM Corporation. The author would like to thank Dr. Thomas Pulliam of the NASA Ames Research Center for providing the block pentadiagonal solver used for comparisons.

References

[1]Jameson, A., Schmidt, W., and Turkel, E., "Numerical Solutions of the Euler Equations by Finite Volume Methods using Runge-Kutta Time-stepping Schemes," AIAA Paper 81-1259, June 1981.

[2]Jameson A., "Solution of the Euler Equations by a Multigrid Method," Mechanical and Aerospace Engineering, Princeton Univ., Princeton, NJ, MAE Rept. 1613, June 1983.

[3]Martinelli, L., Jameson, A., and Grasso, F., "A Multigrid Method for the Navier-Stokes Equations," AIAA Paper 85-0208, Jan. 1985.

[4]Turkel, E., private communication, 1985.

[5]Jameson, A., "Acceleration of Transonic Potential Flow Calculations on Arbitrary Meshes by the Multiple Grid Method," *Proceedings of the AIAA Computational Fluid Dynamics Conference*, AIAA, New York, 1979, pp. 122-146.

[6]Jameson, A. and Yoon, S., "Multigrid Solutions of the Euler Equations Using Implicit Schemes," *AIAA Journal*, Vol. 24, Nov. 1986, pp. 1737-1743.

[7]Chaussee, D. S. and Pulliam, T. H., "Two-Dimensional Inlet Simulation Using a Diagonal Implicit Algorithm," *AIAA Journal*, Vol. 19, Feb. 1981, pp. 153-159.

[8]Jameson, A., "Steady State Solution of the Euler Equations for Transonic Flow," *Transonic, Shock, and Multi-Dimensional Flows: Advances in Scientific Computing*, edited by R. E. Meyer, Academic Press, New York, May 1982, pp. 37-70.

[9]Warming, R. F., Beam, R. M., and Hyett, B. J., "Diagonalization and Simultaneous Symmetrization of the Gas Dynamic Equations," *Mathematics of Computation*, Vol. 29, No. 132, Oct. 1975, pp. 1037-1045.

[10]Briley, W. R. and McDonald, H., "Solution of the Three-Dimensional Compressible Navier-Stokes Equations by an Implicit Technique," *Proceedings of the Fourth International Conference on Numerical Methods in Fluid Dynamics, Lecture Notes in Physics*, Vol. 35, Springer-Verlag, New York, 1974, pp. 105–110.

[11]Beam, R. M. and Warming, R. F., "An Implicit Finite-Difference Algorithm for Hyperbolic Systems in Conservation Law Form," *Journal of Computational Physics*, Vol. 22, No. 1, Sept. 1976, pp. 87–110.

[12]Pulliam, T. H., "Artificial Dissipation Models for the Euler Equations," *AIAA Journal*, Vol. 24, Dec. 1986, pp. 1931–1940.

[13]Rizzi, A., "Numerical Implementation of Solid Body Boundary Conditions for the Euler Equation," Zeitschrift für Angewandte Mathematik und Mechanik, Vol. 58, No. 7, July 1978, pp. 301–304.